ChemPubSoc Europe

DOI: 10.1002/cphc.201500949

CHEMPHYSCHEM Articles

Mechanistic Features of the TiO_2 Heterogeneous Photocatalysis of Arsenic and Uranyl Nitrate in Aqueous Suspensions Studied by the Stopped-Flow Technique

Jorge M. Meichtry,[a, b] Ivana K. Levy,[a, b] Hanan H. Mohamed,[c] Ralf Dillert,[d] Detlef W. Bahnemann,[d, e] and Marta I. Litter*[a, b, f]

The dynamics of the transfer of electrons stored in TiO_2 nanoparticles to As^{III}, As^{V}, and uranyl nitrate in water was investigated by using the stopped-flow technique. Suspensions of TiO_2 nanoparticles with stored trapped electrons (e_{trap}^-) were mixed with solutions of acceptor species to evaluate the reactivity by following the temporal evolution of e_{trap}^- by the decrease in the absorbance at $\lambda = 600$ nm. The results indicate that As^{V} and As^{III} cannot be reduced by e_{trap}^- under the reaction conditions. In addition, it was observed that the presence of As^{V} and As^{III} strongly modified the reaction rate between O_2 and e_{trap}^-: an increase in the rate was observed if As^{V} was present and a decrease in the rate was observed in the presence of As^{III}. In contrast with the As system, U^{VI} was observed to react easily with e_{trap}^- and U^{IV} formation was observed spectroscopically at $\lambda = 650$ nm. The possible competence of U^{VI} and NO_3^- for their reduction by e_{trap}^- was analyzed. The inhibition of the U^{VI} photocatalytic reduction by O_2 could be attributed to the fast oxidation of U^{V} and/or U^{IV}.

1. Introduction

As is very well known, the basic mechanism of TiO_2 heterogeneous photocatalysis involves the formation of electron–hole pairs after band-gap excitation of the semiconductor particles, followed by reductive or oxidative reactions with species present at the water–semiconductor interface. Reductive reactions are less studied than oxidative processes, and some aspects of the mechanistic and kinetic features are still worth exploration.

[a] Dr. J. M. Meichtry, Dr. I. K. Levy, Prof. M. I. Litter
Gerencia Química, Comisión Nacional de Energía Atómica
Av. Gral. Paz 1499, 1650 San Martín
Prov. de Buenos Aires (Argentina)
E-mail: litter@cnea.gov.ar

[b] Dr. J. M. Meichtry, Dr. I. K. Levy, Prof. M. I. Litter
Consejo Nacional de Investigaciones Científicas y Técnicas (CONICET)
Av. Rivadavia 1917
1033 Ciudad Autónoma de Buenos Aires (Argentina)

[c] Dr. H. H. Mohamed
Chemistry Department, Faculty of Science, Helwan University
Ain Helwan, Cairo (Egypt)

[d] Dr. R. Dillert, Prof. D. W. Bahnemann
Institut für Technische Chemie, Leibniz Universität Hannover
Callinstrasse 3, 30167 Hannover (Germany)

[e] Prof. D. W. Bahnemann
Laboratory for Nanocomposite Materials, Department of Photonics
Faculty of Physics, Saint-Petersburg State University
Ulianovskaia str. 3, Peterhof, Saint-Petersburg, 198504 (Russia)

[f] Prof. M. I. Litter
Instituto de Investigación e Ingeniería Ambiental
Universidad Nacional de General San Martín, Campus Miguelete
Av. 25 de Mayo y Francia, 1650 San Martín
Prov. de Buenos Aires (Argentina)

Supporting Information and ORCID(s) from the author(s) for this article are available on the WWW under http://dx.doi.org/10.1002/cphc.201500949.

The stopped-flow spectrophotometric technique has been extensively used in kinetic studies, and it is a very powerful tool for kinetic analysis of reactions with half-lives as short as a few milliseconds, as it is not possible to study such reactions by hand mixing of reagents and conventional measurements of concentration and time.[1–4] Inside the stopped-flow apparatus, reactants are rapidly mixed in a chamber, and the flow is stopped with the reactant stream in a flow cell provided with photometric detection, usually UV/Vis and IR spectroscopy, fluorescence, and/or chemiluminescence,[5,6] or, less common, detection by dichroism, refractive index, and EPR or NMR spectroscopy.[7,8] Thus, stopped flow can be useful to study different types of reactions (e.g. complexation, polymerization, etc.)[4,7] and can be applied to detect transient reaction intermediates.[4,9] Recently, the dynamics of the transfer of trapped electrons (e_{trap}^-) (previously generated and stored in TiO_2 nanoparticles by UV irradiation in the presence of an electron donor) to electron acceptors such as O_2, H_2O_2, NO_3^-, and Cr^{VI} was investigated by employing this technique;[10–13] these studies allowed several features of the initial stages of the photocatalytic reactions of these electron acceptors to be explained, which is generally difficult by steady-state experiments. Due to the relevance of the results, it seemed important to make similar studies on other photocatalytic systems. Reductive photocatalytic systems are far less studied than oxidative ones; in addition, most metals commonly react reductively in heterogeneous photocatalysis. Arsenic and uranium, very well known for their effects on human health if present in water for human consumption, were chosen for the present study.

Water pollution by arsenic is a worldwide problem with high impact in the poorest regions of the planet,[14] with over 226 million exposed people.[15] Arsenic is suspected to be

a human carcinogen, and severe health effects (named arsenicosis or HACRE, hidroarsenicismo crónico regional endémico in Latin America) have been observed in populations drinking arsenic-rich water over long periods of time.[14–16] For this reason, the World Health Organization (WHO) recommends no more than 10 $\mu g\,L^{-1}$ of arsenic in drinking water.[16] Although the main source of As pollution is natural, anthropogenic activities such as mining, wood preservation, and medicinal and agricultural use account for widespread As contamination.[14,17]

Uranium is a radioactive element that can be present in water from geogenic or anthropogenic sources, mainly due to mining and nuclear energy activities;[18] other minor applications are in glass-tinting agents, ceramic glazes, catalysts, and military equipment.[18] The WHO guideline value in drinking water set for this pollutant (30 $\mu g\,L^{-1}$) is related to its chemical toxicity, as it causes nephritis and bone cancer.[16,18,19] Uranyl nitrate in nitric acid is formed in the PUREX process, the major chemical technique used to recover uranium from spent nuclear fuel;[20] the separation of U^{VI} from this aqueous solution is an active research field.[20–22]

Several TiO_2 photocatalytic studies have been undertaken for the As and U systems, and most of them have been recently reviewed,[23–26] including contributions from our group.[27–30] Therefore, stopped-flow studies on As^{III}/As^{V} and uranyl nitrate in TiO_2 photocatalytic systems seemed to be very appealing. The results contribute to the analysis of the role of these species as electron acceptors and to the elucidation of the complex mechanisms involved, shedding light on the initial stages of the processes.

2. Results and Discussion

2.1. Storing of Electrons in TiO_2 Nanoparticles

The following processes take place after UV-A irradiation of $n\,TiO_2$ in the presence of HCOOH and in the absence of O_2 [Eqs. (1)–(5)]:

$$n\,TiO_2 + h\nu \rightarrow n\,TiO_2(e_{CB}^- + h_{VB}^+) \quad (1)$$

$$e_{CB}^- + n\,TiO_2 \rightarrow e^-(Ti^{III}) \quad (2)$$

$$HO_{surf}^-/H_2O_{ads} + h_{VB}^+ \rightarrow HO^\bullet(+H^+) \quad (3)$$

$$HCOOH + h_{VB}^+/HO^\bullet \rightarrow COOH^\bullet/CO_2^{\bullet-} + H^+/H_3O^+ \quad (4)$$

$$COOH^\bullet/CO_2^{\bullet-} + n\,TiO_2 \rightarrow e_{CB}^- + CO_2(+H^+) \quad (5)$$

in which e_{CB}^- and h_{VB}^+ are the electrons and holes generated in the conduction band (CB) and valence band (VB) of $n\,TiO_2$, respectively, and $e^-(Ti^{III}) \equiv e_{trap}^-$. The generated h_{VB}^+ or the hydroxyl radicals formed by attack of the holes to adsorbed water or surface hydroxyls [Eq. (3)] oxidize HCOOH to generate $CO_2^{\bullet-}$ [Eq. (4)], a strong reducing species [$E^0(CO_2/CO_2^{\bullet-}) \approx -2.0$ V[1]][31] that can inject electrons into the CB of $n\,TiO_2$ to end in CO_2.[32]

[1] *All reduction potentials in this article are versus the standard hydrogen electrode (SHE).*

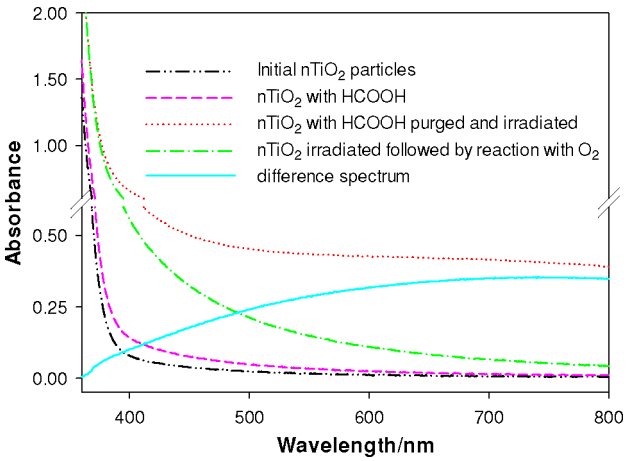

Figure 1. Spectra of $n\,TiO_2$ suspensions under various conditions. Initial $n\,TiO_2$ suspension (3 $g\,L^{-1}$; dashed double dotted black curve), same suspension with 40 mM of HCOOH (dashed pink curve), same suspension with 40 mM HCOOH after 30 min of N_2 bubbling and 24 h irradiation (dotted red curve), irradiated suspension followed by reaction with O_2 (dashed dotted green curve), and absorbance of e_{trap}^- (solid turquoise curve, difference between red and green curves).

Spectra of the $n\,TiO_2$ suspension under different conditions are shown in Figure 1. The dashed double dotted black curve is the initial spectrum of the suspension, whereas the dashed pink curve is the spectrum of the same suspension containing HCOOH and N_2 purged. UV-A irradiation of the suspension leads to accumulation of e_{trap}^-, as can be appreciated in the red dotted curve from the broad absorption increase from $\lambda =$ 510 to 800 nm,[10–13] which does not change after 24 h of irradiation. The generation of stored electrons (e_{trap}^-) was evidenced also by the change in the color of the suspension from transparent to blue. This e_{trap}^--containing suspension was then left open to air, and entering O_2 scavenged the e_{trap}^-, which caused a decrease in the broad band (dotted dashed green curve); in this case, several spectra of this suspension open to air were taken and, once no further variation was observed, it was concluded that all the e_{trap}^- had been scavenged, ensuring total decay.[13] The spectrum of e_{trap}^- is the turquoise curve, obtained by subtracting the red and green curves. The spectra obtained from the 6 $g\,L^{-1}$ $n\,TiO_2$ suspension were very similar (not shown).

The initial e_{trap}^- concentration in $n\,TiO_2$ was determined by direct spectrophotometry at $\lambda = 600$ nm, by using the molar (decadic) absorption coefficient $\varepsilon_{600\,nm} = 600\,M^{-1}\,cm^{-1}$ determined previously.[10,13] From the turquoise curve of Figure 1, an absorbance of 0.32 was obtained for the 3 $g\,L^{-1}$ suspension, corresponding to an e_{trap}^- concentration of 0.53 mM. Assuming that the nanoparticles have a spherical shape with a diameter in the 2–3 nm range,[33] and by using the density of TiO_2 (3.894 $g\,cm^{-3}$ for anatase),[34] an average of about 1–6 electrons per TiO_2 particle can be calculated. For the 6 $g\,L^{-1}$ suspension, an absorbance of 0.35 was obtained (not shown), which corresponds to an e_{trap}^- concentration of 0.59 mM and a similar average value of electrons per TiO_2 particle.

2.2. Stopped-Flow Experiments with Arsenic

In Figure 2, the transients obtained after mixing N_2-purged 0.50 mM As^{III} or As^{V} solutions with a 3 g L^{-1} *n*TiO_2 suspension containing 0.53 mM e_{trap}^- are shown. O_2-saturated water ($[O_2]=0.27$ mM) at pH 2 was used as the reaction test, for which the rapid decay of the absorbance at $\lambda=600$ nm is due to the following reaction [Eq. (6)]:

$$O_2 + e_{trap}^-(+H^+) \rightarrow O_2^{\bullet-}(HO_2^{\bullet}) \quad (6)$$

followed by transformation of $HO_2^{\cdot}$ into H_2O_2, which is then reduced to H_2O by e_{trap}^-.

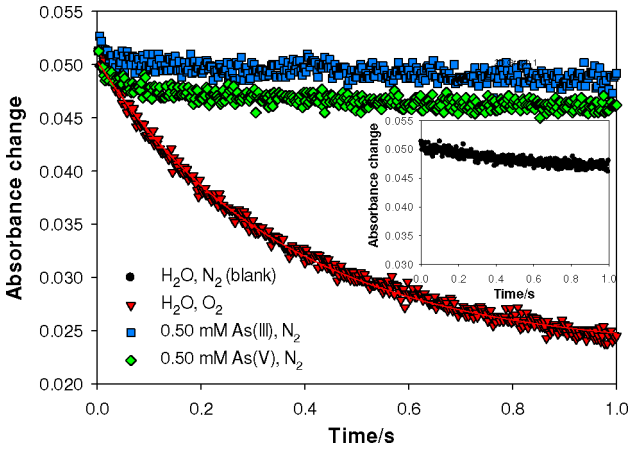

Figure 2. Temporal variation of the $\lambda=600$ nm absorbance (e_{trap}^-) in stopped-flow experiments upon mixing a *n*TiO_2 suspension (3 g L^{-1}) loaded with electrons with As^{III} or As^{V} solutions. Conditions: $[e_{trap}^-]=0.53$ mM, $[As^{III}]_0$ or $[As^{V}]_0=0.50$ mM, pH 2, N_2 purged. The curves of oxygenated water ($[O_2]=0.27$ mM) in the absence of As and the blank of water with N_2 are included. The solid red line shows the fitting of the experimental points of the O_2 decay with e_{trap}^- to Equation (8). Inset: N_2-purged water curve shown alone for clarity.

The decay is almost identical to that obtained in previous experiments for which methanol was used as the donor for the activation of the nanoparticles,[10–12] and this indicates negligible influence of formic acid. Water saturated with N_2 was used as the blank. It can be seen that the decays produced in the presence of 0.50 mM As^{III} and 0.50 mM As^{V} are almost identical to that of the blank, which indicates no reaction between these As species and e_{trap}^-, at least on the studied timescale; this was observed for all the studied As concentrations. The small decay in the absorbance (see inset for the blank) can be attributed to the entrance of small amounts of O_2 into the detection cell of the stopped-flow apparatus within the duration of the measurement. The results of Figure 2 were confirmed by the UV/Vis spectra of the suspensions obtained from the stopping syringe after the end of the measurement in the stopped-flow device (Figure S1 in the Supporting Information). The spectrum after reaction with O_2 is the red curve; no changes in this spectrum were observed after exposure of the suspension to air, which is indicative of complete e_{trap}^- decay. The spectra after reaction with nitrogenated As^{III} and As^{V} solutions are the pink and green curves, respectively, and they are very similar to the spectrum of the blank (black curve), which reveals the presence of e_{trap}^-, that is, the absence of a reaction.[13]

If As^{V} reduction would take place, the first step would be As^{IV} generation [Eq. (7)]:

$$H_3AsO_4 + e^- + H^+ \rightarrow As(OH)_4 \quad (7)$$

The redox level of e_{CB}^- generated in anatase nanoparticles prepared from titanium tetraisopropoxide was reported to be $E^0 \approx -0.5$ V (-0.62 V at pH 2).[35] Assuming that the e_{CB}^- generated in the present *n*TiO_2 (of similar diameter) have the same redox level, and taking into account the standard redox potential of the reaction in Equation (7) ($E^0=-1.2$ V,[36] more negative with the increase in pH), the direct reduction by e_{CB}^- of As^{V} to As^{IV} is not possible. This result was also observed in our previous work,[27] for which reduction of As^{V} by e_{CB}^- generated from P25 was not possible. Reduction of As^{V} by e_{trap}^- stored in the nanoparticles would be less possible, because their reduction potential is proposed to be even less negative, around 0.25 V below the edge of the CB,[35] with reported values ranging from 0.2 to 0.9 V (see Refs. [37, 38] and the references cited therein). Interestingly, As^{V} reduction was actually observed in a study with e_{trap}^- stored in ethanolic TiO_2 nanoparticles.[28] The difference with the present work can be ascribed to different reasons. First, e_{trap}^- generated in the nanoparticles could have different redox potentials because of the different method used to prepare the nanoparticles. Second, a higher number of e_{trap}^- per particle ($\approx$130, see the Supporting Information) exists in the ethanolic nanoparticles, which is reflected by a blueshift in the bandgap (the Burstein–Moss effect); this effect is absent in the present nanoparticles, as it can be appreciated in Figure 1, in which the red and green curves are identical at $\lambda<390$ nm. Third, the reaction between As^{V} and e_{trap}^- is very slow, as reported elsewhere;[39] the effect can be seen in Ref. [28], because a reaction time of at least 30 min is reported, but not in the present stopped-flow experiments, of shorter duration. Therefore, our results confirm those of the previous work,[27] which indicated that As^{V} photocatalytic reduction is only possible if a suitable donor such as methanol is present, as it reacts with holes or hydroxyl radicals to form a strongly reducing radical that can overcome the negative redox potential of the reaction in Equation (7).

Regarding As^{III}, direct reduction by TiO_2 e_{CB}^- was reported in normal photocatalytic experiments,[27] or by electrons stored in ethanolic TiO_2 nanoparticles.[28] The reason for the lack of reaction of As^{III} with e_{trap}^- in the present stopped-flow experiments might be the same as that indicated for As^{V}, that is, a different method used to prepare *n*TiO_2, which gives a different redox potential of the involved e_{trap}^-, a smaller number of e_{trap}^- per particle, or a very slow reaction between As^{III} and e_{trap}^-. It can also be proposed that the reaction does not take place because the redox potential of the reduction of As^{III} to As^{II} is located between that of e_{trap}^- and that of e_{CB}^- (Figure S4); however, this potential is not known and its value should be ob-

tained by electrochemical experiments, which are out of the scope of this article. Another possible explanation for the lack of e_{trap}^- decay is the negligible As^{III} adsorption at pH 2[27,40] required for efficient e_{trap}^- transfer from TiO_2.

Despite these results, it is interesting to study the possible interference of As^{III} or As^{V} on the reaction between e_{trap}^- and O_2. For this, stopped-flow experiments were performed after mixing a saturated O_2 solution (0.27 mM) containing 0.50 mM As^{III} or As^{V} at pH 2 with irradiated nTiO$_2$ ($[e_{trap}^-]=0.53$ mM) (Figure 3). The transients clearly indicate that the presence of As^{III} or As^{V} in the aerated solution affects the rate of electron transfer from e_{trap}^- to O_2 in a different way. On one hand, As^{III} decreases the rate of the $\lambda=600$ nm absorbance change, whereas As^{V} increases this rate, and a complete decay of e_{trap}^- after 0.2 s is observed, as the system arrives to a rather constant absorbance. This is more clearly seen in the inset after 0.005 s (i.e. after the dead time of the equipment), in which a more pronounced slope in the run with As^{V} can be viewed; in contrast, in the experiment with As^{III} (not shown), no reaction was observed on that timescale. The UV/Vis spectra of the suspensions collected from the stopping syringe at the end of the run are shown in Figure S2 and indicate, for the system of O_2 with As^{III}, complete consumption of the e_{trap}^- (see red and blue curves). The spectrum of As^{V} was similar (not shown).

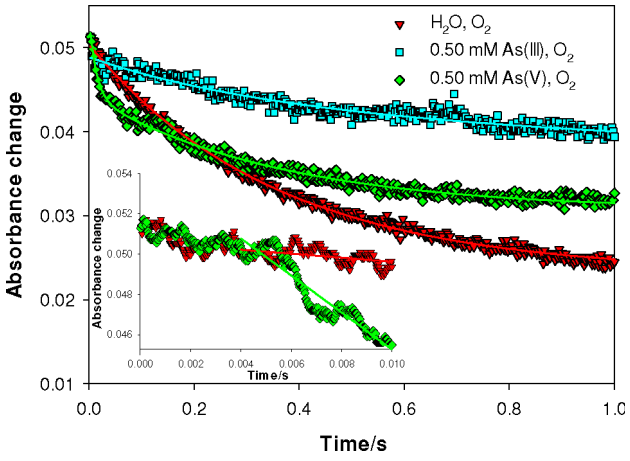

Figure 3. Temporal variation of the $\lambda=600$ nm absorbance (e_{trap}^-) in stopped-flow experiments upon mixing a nTiO$_2$ suspension (3 g L^{-1}) loaded with electrons with oxygenated water solutions in the absence and in the presence of As^{III} and As^{V}. Conditions: $[e_{trap}^-]=0.53$ mM, pH 2, $[O_2]=0.27$ mM, $[As^{III}]_0$ or $[As^{V}]_0=0.50$ mM. Inset: decay at short times (0.01 s). The solid lines show the fitting of the experimental points of H_2O, O_2 without and with 0.50 mM As^{III} with Equation (8), and with 0.50 mM As^{V} with Equation (9); the solid lines in the inset are a linear regression for $t \geq 0.005$ s.

The experimental points of Figures 2 and 3 were fitted to a monoexponential decay [Eq. (8)] for the reaction between O_2 and e_{trap}^- either in the absence of As species (as in Ref. [13]) or in the presence of As^{III}, and to a biexponential decay [Eq. (9)] for the experiments in the presence of As^{V}:

$$\Delta A = \Delta A_0 + \Delta A_1 \times e^{-k_1 t} \quad (8)$$

$$\Delta A = \Delta A_0 + \Delta A_1 \times e^{-k_1 t} + \Delta A_2 \times e^{-k_2 t} \quad (9)$$

in which ΔA_0 is the absorbance change at infinite time, ΔA_1 and ΔA_2 are the absorbance decays due to two different first-order reaction pathways, and k_1 and k_2 are the kinetic constants of each process, with $k_1 > k_2$. Although the monoexponential decay of the reaction between O_2 and e_{trap}^- in the absence of As in the 1 s run suggests the involvement of only one process, experiments performed at longer times (10 s, Figure S3) could be fitted with Equation (9), which indicates that actually two processes take place. The existence of different processes can be explained by adsorption sites of different reactivity or by the existence of electrons of different reducing power, that is, of different reactivity.[37] The fitting parameters are indicated in Table S1, for which the values for the reaction with O_2 are those previously obtained.[13]

All kinetic parameters agree with the above-discussed results. The increase in k_1 from 2.8 to 73 s^{-1} for the run of O_2 in the presence of As^{V} (Table S1) indicates the enhancement in the reaction rate observed in Figure 3, although this decay is too fast to be observed in the 5 s run (Figure S3). The increase in the electron-transfer rate of e_{trap}^- to O_2 by As^{V} can be attributed to the strong adsorption of this species on the TiO_2 surface[40,41] as anionic bidentate complexes,[41] which can decrease both the depth of the e_{trap}^- and the reorganization energy of Equation (6), as reported for organic ligands of high Lewis basicity.[42] The time required for relaxation of the open-circuit potential of irradiated P25 electrodes by O_2 was somewhat faster in the presence of As^{V}[39] (see Figure 2b in Ref. [39]). Analogously, in time-resolved transient absorption spectroscopic studies with aerated P25 suspensions,[43] the decay of e_{trap}^- was slightly faster in the experiments with As^{V} (see Figure 2 in Ref. [43]).

The inhibition of the reaction of e_{trap}^- with O_2 by As^{III} observed in Figure 3 is confirmed by the decrease in ΔA_1 and k_1 and k_2 in the run at 10 s (Table S1). A similar behavior was observed in Ref. [43], in which although As^{III} decreased the amount of generated e_{trap}^- (indicating that it favors electron–hole recombination), the lifetime of the remaining e_{trap}^- was almost constant on the studied timescale (20 μs), which reflects a decrease in the rate of e_{trap}^- transfer to O_2 (see Figure 2 in Ref. [43]). Scavenging of the superoxide/hydroperoxyl radical generated through Equation (6) [or Eq. (10)][44] by As^{III} can account for this inhibition, as this process can reduce the amount of e_{trap}^- that can react with O_2; besides, formed As^{IV} competes with e_{trap}^- for the reaction with O_2 [Eq. (11), $k_{11}=1.4\times10^9$ M^{-1} s^{-1}],[36] which reinforces the inhibition caused by As^{III}. As^{IV} can also inject an electron into the CB [Eq. (12)],[27,45] which thereby decreases e_{trap}^- decay, but this process would be negligible because of the fast reaction of As^{IV} with O_2.[39] Finally, As^{IV} can be reduced by e_{trap}^- to As^{III}[27,46] [Eq. (13), $E^0=+2.4$ V][36] (see Figure S4), which should contribute to e_{trap}^- decay; however, the experimental results clearly reflect that As^{III} decreases the decay rate of e_{trap}^- in the presence of O_2 and, consequently, Equations (10) and (11) represent the preferential reaction mechanism.

$$As^{III} + O_2^{\bullet-} + H^+ \rightarrow As^{IV} + HO_2^- \quad (10)$$

$$As^{IV} + O_2 + H^+ \rightarrow As^V + HO_2^{\bullet} \quad (11)$$

$$As^{IV} \rightarrow As^V + e_{CB}^- \quad (12)$$

$$As^{IV} + e_{trap}^- \rightarrow As^{III} \quad (13)$$

2.3. Stopped-Flow Experiments with Uranium

The results of stopped-flow experiments of a nTiO$_2$ suspension (6 g L^{-1}) loaded with electrons and U^{VI} solutions (0.003–0.250 mM UO_2^{2+} and 0.11–9.5 mM NO_3^-) at pH 2, purged with N_2, are shown in Figure 4. In contrast to the As systems, a significant decay in the signal at $\lambda = 600$ nm was observed.

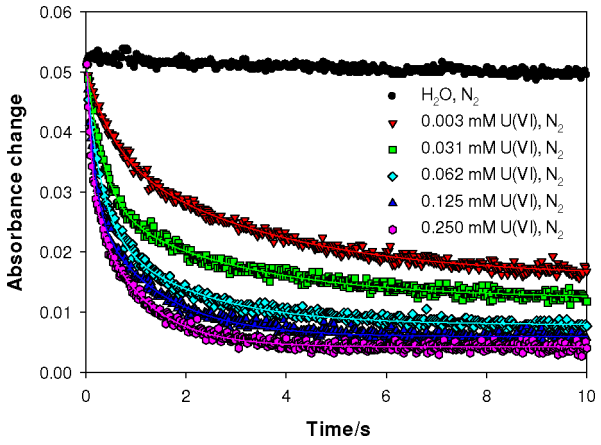

Figure 4. Temporal variation of the $\lambda = 600$ nm absorbance (e_{trap}^-) in stopped-flow experiments upon mixing a nTiO$_2$ suspension (6 g L^{-1}) loaded with electrons with uranyl nitrate solutions. Conditions: [e_{trap}^-] = 0.59 mM, pH 2, U^{VI} solutions at different concentrations ([U^{VI}]:[NO_3^-] 1:38, constant), N_2 purged. The solid lines are the fittings of the experimental points with Equation (9).

In photocatalytic systems, U^{VI} can be reduced by e_{CB}^- to form U^V and U^{IV} as intermediate and final products, in accordance with the redox potentials of the UO_2^{2+}/UO_2^+ and UO_2^+/U^{IV} couples at acid pH values ($E^0 \approx +0.16$ and $+0.38$ V, respectively)[47] relative to that of e_{CB}^- ($E^0 = -0.62$ V at pH 2)[29,30] (see Figure S4). U^{VI} can also be reduced by e_{trap}^- (redox level 0.25 V more positive than that of e_{CB}^-) [Eqs. (14) and (15)].[35]

$$UO_2^{2+} + e_{trap}^- \rightarrow UO_2^+ \quad (14)$$

$$UO_2^+ + e_{trap}^- \rightarrow U^{IV} \quad (15)$$

A direct absorbance measurement by stopped flow of U^{VI}, U^V, and U^{IV} could have been performed to confirm U^{VI} reduction, but the rather small absorbance of these species at $\lambda =$ 380–800 nm hampered this determination.[29,30] Thus, separately, the spectrum of a suspension prepared by mixing equal volumes of a 6 g L^{-1} nTiO$_2$ suspension containing 0.59 mM e_{trap}^- and a deaerated 0.250 mM U^{VI} solution ([NO_3^-] = 9.5 mM), both at pH 2, was recorded, together with those of the separate components (Figure 5).

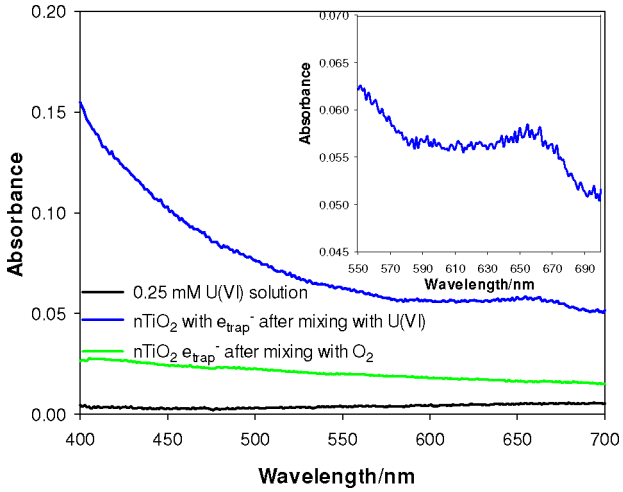

Figure 5. UV/Vis spectra of a mixture of equal volumes of nTiO$_2$ suspension (6 g L^{-1}) containing e_{trap}^- (0.59 mM) and uranyl nitrate solution ([U^{VI}] = 0.250 mM, [NO_3^-] = 9.5 mM) at pH 2 and N_2 purged (blue curve), the uranyl nitrate solution (black curve), and the irradiated nTiO$_2$ suspension after mixing with O_2 saturated solution ([O_2] = 0.27 mM) at pH 2 (green curve). Inset: detailed view of the $\lambda = 550$–700 nm range of the blue curve.

Although complete e_{trap}^- decay takes place after reaction with either O_2 or U^{VI} (green and blue curves, respectively), the latter exhibits a significant absorbance that cannot be ascribed to unreacted e_{trap}^- (as the spectrum does not change if left in contact with O_2), but to the aggregation of nTiO$_2$,[48] as observed in Figure 1 and in Ref. [13], increased by the higher ionic strength caused by the high nitrate concentration (9.5 mM). The presence of U^{IV} is indicated by a new wide signal at $\lambda = 650$ nm (more visible in the inset),[29,30] which confirms U^{VI} reduction. Here, U^{IV} does not precipitate as an oxide because of the formation of a complex with formic acid remaining from the e_{trap}^- storing process,[30] and its detection in solution is possible.

All decays presented in Figure 4 can be accurately adjusted with biexponential Equation (9), according to the occurrence of two different processes, similarly to that explained for Figure 3. The kinetic parameters obtained by regression of the experimental data are summarized in Table 1.

It can be observed that, generally, the total decay ($\Delta A_1 + \Delta A_2$) and the kinetic constants (k_1 and k_2) increase with the concentration of U^{VI}. Interestingly, for the experiment at the lowest concentration of U^{VI} (0.003 mM), the decrease in the absorbance ($\Delta A_1 + \Delta A_2 = 0.0349$) seems to be very high: according to Equations (14) and (15), an equivalent of 0.006 mM e_{trap}^- should be consumed, with corresponding $\Delta A_1 + \Delta A_2 = 0.00036$ (using $\varepsilon_{600\,nm} = 600\ M^{-1}\,cm^{-1}$,[10] 0.2 cm as the optical path, and taking into account the 1:2 dilution factor), a smaller value than the detection limit of the stopped-flow apparatus (0.001). Therefore, the unexpected greater decrease in the signal has to be attributed to the reaction of e_{trap}^- with NO_3^- present in the system ([NO_3^-] = 0.11 mM). In fact, from Equation (16), second-order rate constants for the reaction of NO_3^- with e_{trap}^-, $k^{obs}{}_1$ and $k^{obs}{}_2$ of 1.8×10^4 and $2.8 \times 10^3\ M^{-1}s^{-1}$, respectively, can be calculated, values that are very similar to

Table 1. Kinetic parameters extracted from the fittings of the experimental points of Figure 4 with Equation (9).

Concentration U^{VI} [mM]	ΔA_0	ΔA_1	k_1 [s^{-1}]	ΔA_2	k_2 [s^{-1}]	R^2
0.003	0.0158 ± 0.0001	0.0128 ± 0.0001	1.9 ± 0.1	0.0221 ± 0.0002	0.31 ± 0.01	0.993
0.031	0.0122 ± 0.0001	0.0237 ± 0.0003	2.9 ± 0.1	0.0160 ± 0.0002	0.36 ± 0.01	0.990
0.062	0.0079 ± 0.0001	0.0247 ± 0.0002	3.3 ± 0.1	0.0177 ± 0.0002	0.55 ± 0.01	0.991
0.125	0.0059 ± 0.0001	0.0264 ± 0.0005	6.4 ± 0.1	0.0219 ± 0.0002	0.75 ± 0.01	0.990
0.250	0.0042 ± 0.0001	0.0262 ± 0.0006	9.4 ± 0.2	0.0256 ± 0.0002	1.01 ± 0.01	0.992

those previously reported for the reaction of e_{trap}^- with NO_3^- [Eq. (16)].[12]

$$k = k^{obs} \times [\text{electron acceptor}] \quad (16)$$

However, the values of k^{obs}_1 and k^{obs}_2 obtained with this equation at higher concentrations ($[NO_3^-] \geq 1.17$ mM, $[U^{VI}] \geq 0.031$ mM) are one order of magnitude smaller than those reported in Ref. [12]; nonetheless, the highest concentration of NO_3^- used in that work was 0.25 mM, and only our run with $[U^{VI}] = 0.003$ mM ($[NO_3^-] = 0.114$ mM) lies within the range studied by the authors.

Our previous studies indicate that U^{VI} is reduced in preference to NO_3^- under conventional TiO_2 photocatalytic experiments, either by e_{CB}^- or by reductive organic radicals.[29] In fact, reduction of nitrate by e_{CB}^- is not possible in common photocatalytic systems in the absence of an adequate electron donor[26,49–51] because of the very negative redox potential of the NO_3^-/NO_3^{2-} couple ($E^0 = -0.89$ V)[52] (see Figure S4). However, under conditions similar to those employed here, NO_3^- reduction by e_{trap}^- has been reported.[12,53] A possible explanation is that the redox level of the NO_3^-/NO_3^{2-} couple is more positive than −0.89 V on the TiO_2 surface, which enables NO_3^- reduction; the difference in the present results relative to those of normal photocatalytic conditions can be explained because NO_3^{2-} would be very easily oxidized back to NO_3^- by h_{VB}^+ and/or $HO^{\cdot}$, strong oxidants that are absent in the stopped-flow experiments. Also, it can be proposed that the accumulation of several e_{trap}^- per particle could shift their redox potential to more negative values,[28] which would make NO_3^- reduction feasible. Multielectronic processes will be not considered, because, as recently reported,[54] "no spectroscopic evidence exists so far for multielectron-transfer process in a semiconductor photocatalyst system", in line with our observations in several photocatalytic reactions.[24–26]

At $[U^{VI}] = 0.031$ mM, the NO_3^- concentration is in excess with respect to the total amount of e_{trap}^- (1.18 mM vs. 0.59 mM), and complete e_{trap}^- decay should therefore be expected. However, at higher concentrations of U^{VI}, the absorbance change increases (see Figure 4 and $\Delta A_1 + \Delta A_2$ in Table 1). Therefore, it can be inferred that only a fraction of e_{trap}^- reacts with NO_3^-. As the number of e_{trap}^- per particle decreases due to this reaction, the redox potential of the remaining e_{trap}^- would also decrease until NO_3^- can no longer be reduced. The fate of remaining e_{trap}^- cannot be predicted, as they could react with U^{VI} or N species formed after NO_3^{2-} hydrolysis, such as NO_2[52] and nitrite.[31]

As reported, the presence of O_2 strongly inhibits U^{VI} photocatalytic reduction.[18,30,55] Noticeably, the rate constants k_1 and k_2 of Tables S1 and 1 and of Ref. [13] for systems having similar concentrations of electron acceptors ($[O_2] = 0.27$ mM and $[U^{VI}] = 0.25$ mM) are higher for U^{VI}. Therefore, it can be proposed that the inhibition by O_2 in the U^{VI} photocatalytic reduction is due to the fast oxidation of U^V and/or U^{IV} to U^{VI} and not to faster capture of e_{CB}^- by O_2. This elucidates the dichotomy proposed years ago by Chen et al.[55] concerning whether or not, in photocatalytic systems, dissolved oxygen is either a better electron scavenger than uranyl or a strong oxidant by which the reduced uranyl species can be rapidly reoxidized.

3. Conclusions

The results herein obtained indicate that no reaction takes place between trapped electrons (e_{trap}^-) and As^V or As^{III} within the studied timescale (up to 10 s). This reinforces previous reports that indicate that As^V cannot be reduced by TiO_2 electrons. Although As^{III} was actually found to be reduced by electrons generated in the conduction band (e_{CB}^-) in normal photocatalytic studies or by electrons stored in ethanolic TiO_2 nanoparticles, the present results can be explained by the different characteristics of the TiO_2 samples, the different redox potential of e_{trap}^- present in each system, and a very slow reaction rate of As^{III} as electron acceptor.

In addition, the presence of As^V and As^{III} dramatically modifies the reaction rate between O_2 and e_{trap}^-, with an increase in the rate if As^V is present and a decrease in the rate caused by the presence of As^{III}. In the case of As^V, this can be due to the strong adsorption of As^V on the TiO_2 surface, which can decrease the depth of the e_{trap}^-. The effect of As^{III} in decreasing e_{trap}^- decay was attributed to a complex mechanism involving multiple steps with the participation of hydroperoxyl radicals and scavenge of O_2 by As^{IV}.

In contrast with As, U^{VI} was observed to react easily with e_{trap}^-. NO_3^- and U^{VI} reduction take place simultaneously, although U^{VI} is reduced in preference, as previously reported. The formation of U^{IV} was observed in the spectrum of the nanoparticles mixed with U^{VI} at $\lambda = 650$ nm. An important observation of the results is that the inhibition by O_2 in the U^{VI} photocatalytic reduction can be attributed to the fast oxidation of U^V and/or U^{IV} to U^{VI} and not to a faster capture of e_{CB}^- by O_2, which sheds light onto this dichotomy.

Experimental Section

Materials and Chemicals

All chemicals were of the highest available purity and were used as received: $TiCl_4$ (99.9%), $NaNO_3$ (99.995%), and H_2O_2 (30%) were purchased from Sigma–Aldrich; $NaAsO_2$ and $Na_2HAsO_4{\cdot}7H_2O$ were purchased from Baker; and formic acid (HCOOH) was obtained from Merck. For U^{VI}, a 1000 mg L^{-1} uranyl standard solution for atomic absorption in 1.06% *w/w* HNO_3 (Fluka) was used. For pH adjustments, 1 M HCl (Merck) was used. All solutions and suspensions were prepared with deionized water from a Sartorius Arium 611 apparatus (resistivity = 18.2 MΩ cm^{-1}).

The transparent TiO_2 nanoparticles (*n*TiO_2, 2–3 nm particle size) were prepared as previously reported.[10–13] Briefly, a solution of $TiCl_4$ (3.5 mL), prechilled to −20 °C, was added slowly to deionized water (900 mL) at 1 °C under vigorous magnetic stirring. After continuous stirring for 1 h, the resulting colloidal suspension was dialyzed against deionized water by using a double dialysis membrane up to a final pH between 2 and 3. The solution was kept at 5 °C for around 12 h under stirring, and the solvent was removed under reduced pressure at 2.0–2.5 kPa and 27–30 °C. Off-white shining crystals were obtained, which were resuspended in pure water to obtain perfectly transparent colloidal TiO_2 suspensions.

Storing of Electrons in TiO_2 Nanoparticles

The production of e_{trap}^- used in the experiments with As^V and As^{III} was performed similarly to that described in Refs. [10,13] Briefly, a *n*TiO_2 suspension (3 g L^{-1}, by diluting the 6 g L^{-1} suspension indicated above) containing 40 mM HCOOH at pH 2 was poured into a glass cell (51 mL) provided with a sealed silicone cap, and was bubbled with N_2 for 30 min at 0.5 L min^{-1} to ensure removal of dissolved O_2. Then, the suspension was irradiated with an OSRAM HBO-500W high-pressure Hg lamp, with a quartz water filter to avoid IR radiation (UV-A intensity 2.6×10^{-3} J cm^{-2} s^{-1}, measured with an LTLutron UVA-365 UV radiometer). For storing electrons in *n*TiO_2 for the U^{VI} experiments, the 6 g L^{-1} *n*TiO_2 suspension with 40 mM HCOOH was placed inside a quartz cell equipped with a cooling water jacket and was irradiated with a Phillips UV-A ($\lambda >$ 300 nm, UV-A intensity 2.1×10^{-3} J cm^{-2} s^{-1}) Original Home Solaria sun bed. In all cases, irradiation of the *n*TiO_2 suspension was performed up to 24 h, although no significant changes in the absorbance were observed after 120 min of irradiation, which indicated that the maximum e_{trap}^- storage capacity was obtained.

Stopped-Flow Experiments

Stopped-flow experiments were performed by using the same equipment and conditions as those described before.[13] Briefly, an SX.18MV-R rapid mixing spectrophotometer (Applied Photophysics), with a 2 mm optical path cell, was used. The dead time of the equipment was about 5 ms, and the residence time in the mixing cell was around 4 ms, with a receptor syringe volume of 500 μL that received the liquid from 1000 μL injection syringes; once the receptor syringe was filled, the injection of the solutions was arrested and the measurement was started. The detection light was obtained from a Spectra Kinetic Monochromator, operative between 200 and 700 nm, and by using a 100 W tungsten incandescent lamp as the light source.

The concentration of As^{III} and As^V for the stopped-flow experiments was in the range of 0.005 to 0.50 mM, whereas for U^{VI}, the solutions were in the range of 0.003 to 0.250 mM UO_2^{2+} (containing 0.11-9.5 mM NO_3^-). These concentrations were similar to those used in previous stopped-flow experiments.[10–13] All solutions were adjusted to pH 2; this pH was chosen to assure that the nanoparticles presented very little aggregation and were thus stable enough for the stopped-flow experiments. In anoxic experiments, N_2 was bubbled into the solution for at least 15 min at 0.5 L min^{-1} ($[O_2] \leq$ 0.1 mg L^{-1}), whereas in the experiments with O_2, the solution was left open to air under magnetic stirring for at least 30 min ($[O_2] \approx$ 8.6 mg L^{-1}). In a typical stopped-flow experiment, a *n*TiO_2 suspension loaded with electrons was carefully filled into one syringe and the solution containing the electron acceptor (As^V, As^{III}, U^{VI}, or O_2) was filled into another one. The solutions were injected into the mixing chamber (1:1 *v/v*), and the resulting mixture was led to the optical cell, in which the temporal change in the absorbance at λ = 600 nm was measured.

All stopped-flow determinations were performed in triplicate, and the results were averaged, with relative standard deviations smaller than 5%. The fitting of the experimental points was made with Origin 8.0 software, with reduced χ^2 as the iteration-ending criterion.

Analytical Spectrophotometric Determinations

The UV/Vis spectra and the analytical spectrophotometric determinations over the λ = 200–800 nm range were recorded by employing a Varian Cary 100 Scan UV/Vis system in a quartz cell of 1 cm optical path.

Acknowledgements

This work was performed as part of Agencia Nacional de Promoción Científica y Tecnológica PICT-0463 and Consejo Nacional de Investigaciones Científicas y Técnicas–Deutsche Forschungsgemeinschaft (CONICET-DFG) 183/13 projects.

Keywords: arsenic · heterogeneous catalysis · photocatalysis · stopped flow · uranium

[1] P. M. Beckwith, S. R. Crouch, *Anal. Chem.* **1972**, *44*, 221–227.
[2] A. Gomez-Hens, D. Perez-Bendito, *Anal. Chim. Acta* **1991**, *242*, 147–177.
[3] A. Loriguillo, M. Silva, D. Pérez-Bendito, *Anal. Chim. Acta* **1987**, *199*, 29–40.
[4] T. Pérez-Ruiz, C. Martínez-Lozano, V. Tomás, J. Fenoll, *Analyst* **2000**, *125*, 507–510.
[5] H. A. Mottola, *Kinetic Aspects of Analytical Chemistry*, Wiley, New York, **1988**, pp. 172–178.
[6] R. A. Harvey, W. O. Borcherdt, *Anal. Chem.* **1972**, *44*, 1926–1928.
[7] M. D. Christianson, E. H. P. Tan, C. R. Landis, *J. Am. Chem. Soc.* **2010**, *132*, 11461–11463.
[8] D. B. Green, J. Lane, R. Wing, *Appl. Spectrosc.* **1987**, *41*, 847–851.
[9] D. A. Couch, O. W. Howarth, P. Moore, *J. Chem. Soc. Chem. Commun.* **1975**, 822–823.
[10] H. H. Mohamed, R. Dillert, D. W. Bahnemann, *J. Photochem. Photobiol. A* **2011**, *217*, 271–274.
[11] H. H. Mohamed, R. Dillert, D. W. Bahnemann, *J. Phys. Chem. C* **2011**, *115*, 12163–12172.
[12] H. H. Mohamed, C. B. Mendive, R. Dillert, D. W. Bahnemann, *J. Phys. Chem. A* **2011**, *115*, 2139–2147.
[13] J. M. Meichtry, R. Dillert, D. W. Bahnemann, M. I. Litter, *Langmuir* **2015**, *31*, 6229–6236.
[14] M. I. Litter, M. E. Morgada, J. Bundschuh, *Environ. Pollut.* **2010**, *158*, 1105–1118.

[15] S. Murcott, *Arsenic Contamination in the World—An International Sourcebook*, IWA, London, **2012**.
[16] WHO, *Guidelines for Drinking-Water Quality, 4th ed.*, World Health Organization, Geneva, **2011**.
[17] L. S. Keith, O. M. Faroon, B. A. Fowler, *Handbook on the Toxicology of Metals, 4th ed.* (Eds.: G. F. Nordberg, B. A. Fowler, M. Nordberg), Elsevier, London, **2015**, pp. 1307 – 1345.
[18] *Uranium in the Aquatic Environment* (Eds.: B. Merkel, B. Planer-Friedrich, C. Wolkersdorfer), Springer, Berlin, **2002**, p. 200.
[19] E. Ansoborlo, L. Lebaron-Jacobs, O. Prat, *Environ. Int.* **2015**, *77*, 1 – 4.
[20] G. Kessler, *Proliferation-Proof Uranium, Plutonium Fuel Cycles: Safeguards and Non-proliferation*, Kit Scientific Publishing, Karlsruhe, **2011**, p. 107.
[21] H. Jingxin, Z. H. Xianye, D. Yunfu, Z. Zhihong, X. Honggui, *J. Less-Common Met.* **1986**, *122*, 287 – 294.
[22] T. Chikazawa, T. Kikuchi, A. Shibata, T. Koyama, S. Homma, *J. Nucl. Sci. Technol.* **2008**, *45*, 582 – 587.
[23] M. I. Litter, *Appl. Catal. B* **1999**, *23*, 89 – 114.
[24] M. I. Litter, *Adv. Chem. Eng.* **2009**, *36*, 37 – 67.
[25] M. I. Litter, *Pure Appl. Chem.* **2015**, *87*, 557 – 567.
[26] M. I. Litter, N. Quici, J. M. Meichtry, A. M. Senn, "Photocatalytic removal of metallic and other inorganic pollutants" in *Photocatalysis*: *Fundamentals and Perspectives* (Eds.: J. Schneider, D. Bahnemann, J. Ye, J. Li, G. Puma, D. D. Dionysiou), Royal Society, London, **2016**, in press.
[27] I. K. Levy, M. Mizrahi, G. Ruano, F. Requejo, G. Zampieri, M. I. Litter, *Environ. Sci. Technol.* **2012**, *46*, 2299 – 2308.
[28] I. K. Levy, M. A. Brusa, M. E. Aguirre, G. Custo, E. S. Román, M. I. Litter, M. A. Grela, *Phys. Chem. Chem. Phys.* **2013**, *15*, 10335 – 10338.
[29] V. N. Salomone, J. M. Meichtry, G. Zampieri, M. I. Litter, *Chem. Eng. J.* **2015**, *261*, 27 – 35.
[30] V. N. Salomone, J. M. Meichtry, M. I. Litter, *Chem. Eng. J.* **2015**, *270*, 28 – 35.
[31] P. J. Wardman, *J. Phys. Chem. Ref. Data* **1989**, *18*, 1637 – 1755.
[32] L. L. Perissinotti, M. A. Brusa, M. A. Grela, *Langmuir* **2001**, *17*, 8422 – 8427.
[33] C. Kormann, D. W. Bahnemann, M. R. Hoffmann, *J. Phys. Chem.* **1988**, *92*, 5196 – 5201.
[34] J. K. Burdett, T. Hughbanks, G. J. Miller, J. W. Richardson, J. V. Smith, *J. Am. Chem. Soc.* **1987**, *109*, 3639 – 3646.
[35] S. T. Martin, H. Herrmann, M. R. Hoffmann, *J. Chem. Soc. Faraday Trans.* **1994**, *90*, 3323 – 3330.
[36] U. K. Kläning, B. H. J. Bielski, K. Sehested, *Inorg. Chem.* **1989**, *28*, 2717 – 2724.
[37] N. Serpone, D. Lawless, R. Khairutdinov, *J. Phys. Chem.* **1995**, *99*, 16646 – 16654.
[38] L. Zhang, H. H. Mohamed, R. Dillert, D. Bahnemann, *J. Photochem. Photobiol. C* **2012**, *13*, 263 – 276.
[39] D. Monllor-Satoca, R. Gómez, W. Choi, *Environ. Sci. Technol.* **2012**, *46*, 5519 – 5527.
[40] H. Yang, W.-Y. Lin, K. Rajeshwar, *J. Photochem. Photobiol. A* **1999**, *123*, 137 – 143.
[41] M. Pena, X. Meng, G. P. Korfiatis, C. Jing, *Environ. Sci. Technol.* **2006**, *40*, 1257 – 1262.
[42] J. Moser, S. Punchihewa, P. Infelta, M. Grätzel, *Langmuir* **1991**, *7*, 3012 – 3018.
[43] W. Choi, J. Yeo, J. Ryu, T. Tachikawa, T. Majima, *Environ. Sci. Technol.* **2010**, *44*, 9099 – 9104.
[44] T. Xu, P. V. Kamat, K. E. O'Shea, *J. Phys. Chem. A* **2005**, *109*, 9070 – 9075.
[45] E. C. Dutoit, F. Cardon, W. P. Gomes, *Ber. Bunsen-Ges. Phys. Chem.* **1976**, *80*, 1285 – 1288.
[46] J. Ryu, W. Choi, *Environ. Sci. Technol.* **2006**, *40*, 7034 – 7039.
[47] L. Martinot, J. Fuger, "The Actinides" in *Standard Potentials in Aqueous Solution* (Eds.: A. J. Bard, R. Parsons, J. Jordan), Marcel Dekker, New York, **1985**, pp. 631 – 674.
[48] J. Sun, L.-H. Guo, H. Zhang, L. Zhao, *Environ. Sci. Technol.* **2014**, *48*, 11962 – 11968.
[49] J. Sá, C. A. Agüera, S. Gross, J. A. Anderson, *Appl. Catal. B* **2009**, *85*, 192 – 200.
[50] K. Doudrick, O. Monzón, A. Mangonon, K. Hristovski, P. Westerhoff, *J. Environ. Eng.* **2012**, *138*, 852 – 861.
[51] K. Doudrick, T. Yang, K. Hristovski, P. Westerhoff, *Appl. Catal. B* **2013**, *136*, 40 – 47.
[52] A. R. Cook, N. Dimitrijevic, B. W. Dreyfus, D. Meisel, L. A. Curtiss, D. M. Camaioni, *J. Phys. Chem. A* **2001**, *105*, 3658 – 3666.
[53] R. Gao, A. Safrany, J. Rabani, *Radiat. Phys. Chem.* **2003**, *67*, 25 – 39.
[54] P. V. Kamat, *J. Phys. Chem. Lett.* **2012**, *3*, 663 – 672.
[55] J. Chen, D. F. Ollis, W. H. Rulkens, H. Bruning, *Colloids Surf. A* **1999**, *151*, 339 – 349.

Manuscript received: October 23, 2015
Accepted Article published: December 29, 2015
Final Article published: January 13, 2016